Analyst

Cite this: *Analyst*, 2012, **137**, 3697

www.rsc.org/analyst

PAPER

Fabrication of glutathione photoelectrochemical biosensor using graphene–CdS nanocomposites

Xiaomei Zhao, Shiwei Zhou, Qingming Shen, Li-Ping Jiang and Jun-Jie Zhu*

Received 18th May 2012, Accepted 9th June 2012
DOI: 10.1039/c2an35658a

A novel glutathione (GSH) photoelectrochemical biosensor was fabricated using the newly synthesized graphene–CdS (GR–CdS) nanocomposites. The GR–CdS nanocomposites were prepared by a fast, one-step, aqueous reaction. The as-prepared GR–CdS structure inherited the excellent electron transport of GR and facilitated the spatial separation of photo-generated charge carrier, therefore resulting in the enhanced photocurrent, and making it a promising candidate for developing photoelectrochemical biosensors. The proposed GSH sensor displays satisfactory analytical performance with an acceptable linear range from 0.01 to 1.5 mmol L^{-1} with a detection limit of 0.003 mmol L^{-1} at a signal-to-noise ratio of 3, and also shows an excellent specificity against anticancer drugs and can be successfully applied for GSH detection in real samples. The as-synthesized GR–CdS nanocomposites exhibited obviously enhanced photovoltaic properties, which could be extended to the detection of other enzymes and biomolecules, thus providing a promising platform for the development of photoelectrochemical biosensors.

Introduction

Glutathione (GSH), a thiol-containing tripeptide (γ-L-glutamyl-L-cysteinyl-glycine), as the most abundant non-protein, low-molecular-weight thiol source in most mammalian tissues, plays an important role in many biological functions involving antioxidant defense, signal transduction, and cell proliferation.[1–4] Upon oxidation, GSH is transformed to glutathione disulfide (GSSG). The concentrations of GSH and GSSG and their molar ratio are indicators of cell functionality and oxidative stress.[5] Thus, based on the biological importance of GSH, many strategies have been developed for the quantification of GSH.[5–12]

As a newly developed technique for the detection of biomolecules, photoelectrochemical measurement has attracted more and more interest.[13–16] In the case of the photoelectrochemical detection process, light is used to excite active species on the electrode, and current is used as the detection signal, which is just the reverse process of electrochemiluminescence. Benefiting from the different forms of energy for excitation and detection, its sensitivity and specificity could potentially match that of electrochemiluminescence.[14] In addition, the use of electronic readout makes the instrument simpler, cheaper, and easier to miniaturize than that of optical methods. Coupling photoirradiation with an electrochemical system, photoelectrochemical sensors have the advantages of both optical and electrochemical methods.[17,18] Thus, this technique shows promising analytical applications and has attracted considerable interest. Nowadays, more and more new materials with excellent optoelectronic properties were prepared for various high-performance photovoltaic devices.[13,19–27]

Traditionally, semiconductor nanoparticles have been regarded as attractive candidates for photoelectric applications due to their size-tunable optical and electronic properties, as well as their efficient multiple charge carrier generations. To enhance the photocurrent generated by the semiconductor materials, it is essential to retard the recombination of electron–hole species in the semiconductors by molecular electron-relay semiconductor structures or efficient electron-transport matrices, such as conductive polymer films or carbon nanotubes (CNTs).[22–25] The assembly of semiconductors on these matrices has been extensively studied for their promising optoelectronic applications.[23–27] Graphene (GR), for its zero band gap and high electron mobility (15 000 cm^2 V^{-1} s^{-1}),[28] has been extensively considered as a promising candidate for an electron acceptor and transport matrix.[29] The incorporation of GR in photovoltaic devices can enhance the charge separation and facilitate the charge transport, and thus improve the photovoltaic performances, which has attracted more and more interest. Some GR based optoelectronic systems have been reported.[30–33] CdS is one of the most widely studied semiconductors as a photoanode in photoelectrochemical cells due to its excellent photoelectrochemical propeties.[14,31–33] Herein, we reported a novel, facile, one-step synthetic route for graphene–CdS nanocomposites that showed promising optoelectronic properties, as illustrated in Scheme 1. In this reaction the reduction of GO and

State Key Laboratory of Analytical Chemistry for Life Science, School of Chemistry and Chemical Engineering, Nanjing University, Nanjing, 210093, P.R. China. E-mail: jjzhu@nju.edu.cn; Fax: +86-25-8359-7204; Tel: +86-25-8359-7204

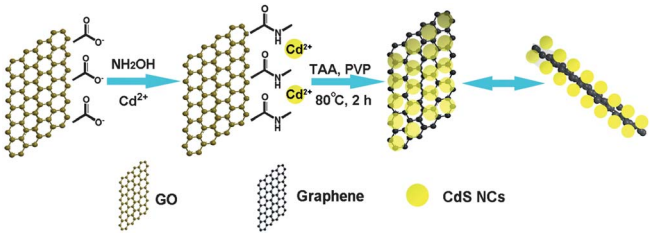

Scheme 1 Schematic illustration of the one-step synthesis of GR–CdS nanocomposites.

the deposition of CdS nanocrystals (NCs) on GR nanosheets was performed simultaneously. The novel route for the fabrication of GR–CdS was based on the modification of our previous work.[33] It is worth mentioning that the introduction of hydroxylamine (NH_2OH) facilitated the coordination with cadmium, enriching much more cadmium ions on the GO sheets, and more nucleation sites were formed, which made a higher-coverage of CdS nanocrystals on the GR sheets. In addition, in the presence of NH_2OH, it also contributed to the assisted reduction of GO and the stabilization of CdS NCs *via* attachment with the negatively charged $–COO^-$ and $–OH^-$ groups on GO.[34–36] The good crystalline structure and dispersion of the obtained GR–CdS nanocomposites endowed them with enhanced photoelectric properties. The size and crystalline phase of CdS NCs in this work were different from our previous work, and the uniform and small size led to a higher-coverage of CdS on GR sheets so that an enhanced photocurrent was observed at the same measurement conditions as before.[33] In the basis of the efficient photoelectrochemical performance of the GR–CdS nanocomposites, a sensitive biosensor was successfully fabricated for the detection of GSH, which showed good performance in the monitoring of GSH with a rapid response, wide concentration range, low detection limit and good selectivity. It could successfully be applied to real sample detection of Isethion (Tathion eye drops). The GR–CdS nanocomposites provided a robust approach for the photoelectrochemical detection of biomolecules.

Experimental

Materials and reagents

All chemicals were obtained from commercial sources and used without further purification. Graphite powder (KS-10) and hydroxylamine solution (NH_2OH, 50 wt% in H_2O, 99.999%) were purchased from Sigma-Aldrich (St. Louis, MO). Reduced L-glutathione (GSH, 99%) was from Aladdin Chemistry Co. Ltd. Polyvinylpyrrolidone (PVP, K-30) was purchased from Sinopharm Chemical Reagent Co., Ltd (Shanghai, China), $CdCl_2 \cdot 2.5H_2O$ (99%) was from Shanghai Jinshanting New Chemical Reagent Co., Ltd (China) and thioacetamide (TAA, ≥99%) was from Lingfeng Chemical Reagent Co., Ltd (Shanghai, China). All other reagents were of analytical grade and were used without further purification. All aqueous solutions were prepared using ultrapure water (Milli-Q, Millipore). Phosphate buffer solution (PBS, 0.1 mol L^{-1}, pH = 7.0) was always employed as the supporting electrolyte after being de-aerated with high-purity nitrogen. Tathion eye drops (Isethion, 5 mL/100 mg) was from ISEI Company, Incorporated, Japan.

Instrument

High-resolution transmission electron microscopy (HR-TEM) images were measured on a JEOL 2100 transmission electron microscope using an accelerating voltage of 200 kV. The specimens were prepared by placing two drops of the solution with dispersed nanoparticles on a carbon film coated copper grid (400 mesh) and then dried under room temperature. Wide-angle powder X-ray diffraction (XRD) patterns were obtained with a Philips X'pert Pro X-ray diffractometer (CuKα radiation, λ = 0.15418 nm). The UV-visible (UV-vis) spectrum was recorded using a Shimadzu UV-3600 UV-visible spectrophotometer. Fourier transform infrared (FT-IR) spectra were obtained using a Bruker Vector 22 spectrometer in the frequency range of 4000–500 cm^{-1}. Photoelectrochemical measurements were performed with a home-built photoelectrochemical system. A 500 W Xe lamp equipped with a monochromator was used as the irradiation source to produce the monochromatic illuminating light. The photocurrent intensity was recorded on a CHI 660D electrochemical workstation (Shanghai Chenhua Apparatus Corporation, China) with a three-electrode system. In the system, a modified ITO electrode (0.5 cm × 0.5 cm) was used as the working electrode, a Pt wire was used as the counter electrode and an Ag/AgCl electrode was used as the reference electrode. All the photocurrent measurements were carried out in PBS (0.1 M, pH 7.0), which was de-aerated by highly pure nitrogen for 15 min before experiments and then kept over a N_2 atmosphere for the entire experimental process. The applied potential was 0 V (*versus* Ag/AgCl) and the light wavelength was 470 nm.

Synthesis of GR–CdS nanocomposites

Graphite oxide (GO) was prepared from graphite powder by a modified Hummers method,[37] and then dispersed into water to yield a yellow brown dispersion by ultrasonication for 2 h, followed by centrifugation at 3000 rpm for 20 min to remove unexfoliated GO. In order to prepare GR–CdS nanocomposites, GO dispersion (200 μL, 0.5 mg mL^{-1}) with 1.3 μL of NH_2OH and 0.2 g of PVP were dispersed into twice-distilled water (50 mL). After vigorous stirring, 0.114 g $CdCl_2 \cdot 2.5H_2O$ and 0.1 g TAA were added. The obtained solution was then reacted at 80 °C for 2 h under vigorous stirring. Finally, the product was centrifuged at 9000 rpm, and dried in a vacuum drier. As a control, the free GR and CdS NCs were also prepared under the same reaction conditions without adding $CdCl_2 \cdot 2.5\ H_2O$ or GO, respectively.

Results and discussion

Morphology and spectroscopic characterizations

The morphologies of GR–CdS nanocomposites were observed by transmission electron microscopy (TEM). The TEM images (Fig. 1A) show that all of the GR sheets are well decorated with CdS NCs densely and evenly. Neither free GR sheets nor undecorated CdS NCs are observed in this sample. The individual CdS NCs had an average diameter ~6 nm, which were

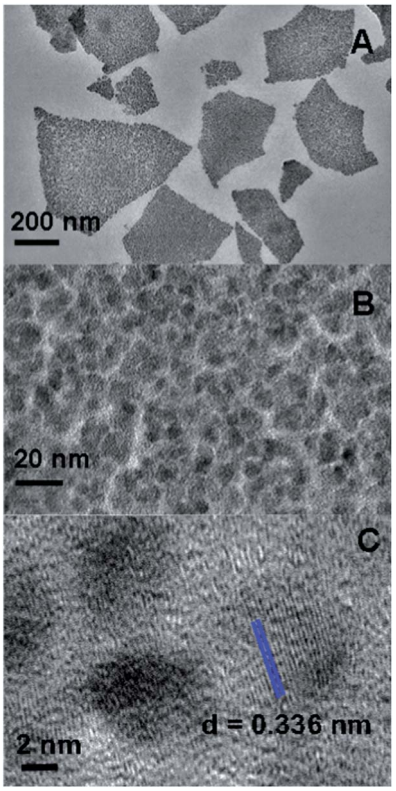

Fig. 1 (A) TEM image of a GR sheet densely coated with CdS NCs. (B) Magnified TEM image of CdS NCs on a GR sheet. (C) High-resolution TEM image of CdS NCs on the GR sheet.

well separated from each other and well spread out on the GR sheets (Fig. 1B). In the HR-TEM image (Fig. 1C), the lattice fringe with interplanar distance is 0.336 nm, which can be assigned to the (100) plane of the cubic CdS. The good distribution and high-coverage of CdS on the GR sheets can guarantee efficient optoelectronic properties of the GR–CdS nanocomposites.

X-Ray diffraction (XRD) measurements were employed for the investigation of the phase and structure. As shown in Fig. 2A, the XRD pattern of the pristine GO (curve a) shows a sharp peak at $2\theta = 10.2°$, corresponding to the (001) reflection of graphite oxide.[38] After the reduction by TAA and NH_2OH, no obvious peaks were observed in the GR (curve b), indicating that GO was reduced completely. All the diffraction peaks of free CdS (curve c) matched well with that of cubic CdS phase (JCPDS no. 65-2887). XRD peaks of the CdS heterostructure in GR–CdS (curve d) show scattering angles of 26.52°, 44.12° and 52.18°, corresponding to crystal planes (111), (220) and (311) of CdS, respectively. The results suggest that CdS NCs decorated on graphene sheets are in cubic zinc blende form.[32] Meanwhile, the broad diffraction peaks in the XRD patterns indicate the size of the CdS is small.

Fig. 2B shows the UV-vis absorption spectra of the samples. The pristine GO shows a strong absorption peak at 230 nm (curve a), while GR shows a characteristic peak at 270 nm (curve b), which is generally regarded as the excitation of the π-plasmon of graphitic structure.[39] The absorption peaks of the free CdS and GR–CdS nanocomposites are at around 450 nm (curve c) and 470 nm (curve d), respectively. Furthermore, in the case of GR–CdS nanocomposites, the absorption peak of GO at about 230 nm disappears, indicating that GO is reduced to GR.

The FT-IR spectra of samples are shown in Fig. 2C. The oxygen-containing functional groups of GO are revealed by the bands at 1750 cm^{-1}, 1410 cm^{-1} and 1245 cm^{-1}, corresponding to C=O stretching of COOH groups, the C–O–H deformation peak and C–OH stretching peak, respectively.[40,41] The peak at 1620 cm^{-1} can be assigned to the vibration of the adsorbed water molecules and the skeletal vibration of unoxidized graphitic domains.[41,42] All of these bands related to the oxygen-containing functional groups almost disappear in the FT-IR spectra of GR and the GR–CdS nanocomposites, revealing that the oxygen-containing functional groups of GO are almost removed by the reduction of TAA with the assistance of NH_2OH, and thus GO was transformed to GR.

The Raman spectrum in Fig. 2D also confirms the reduction of GO. Raman spectrum of the pristine GO displays two prominent peaks at around 1600 cm^{-1} and 1360 cm^{-1}, corresponding to the G and D bands, respectively (curve a). A general feature of the reduction of GO is that the G band shifts to lower wavenumber.[32] In the case of GR and GR–CdS, the G band shifted to 1586 cm^{-1} and 1590 cm^{-1}, respectively, indicating the reduction of GO. Furthermore, an obvious decrease of the D/G ratio in GR and GR–CdS can be observed in comparison with that of GO, also indicating the decrease in the average size of the sp^2 domains upon reduction of the exfoliated GO.[32,40]

Photoelectrochemical oxidation of GSH

The photocurrent generation of the films was studied by employing the modified ITO electrodes as photoanodes. As is shown in Fig. 3A, upon irradiation with light at a wavelength of 470 nm, in 0.1 M PBS (pH 7.0), the CdS/ITO electrode shows a photocurrent of 0.81 μA at an applied potential of 0 V (curve a), whereas the GR–CdS/ITO electrode shows a photocurrent of 1.35 μA (curve b), indicating the improvement of the photocurrent conversion efficiency of CdS by the addition of GR. However, in the blank PBS solution, there were not enough effective electron donors for scavenging of the photogenerated holes. Once there is an effective electron donor for scavenging of the holes, the photocorrosion reaction and the electron–hole recombination are inhibited and the photocurrent intensity can be enhanced. For example, ascorbic acid (AA) was well known as a non-toxic electron donor under a mild solution medium.[14] In this case, 0.1 mol L^{-1} PBS (pH = 7.0) containing 0.1 mol L^{-1} AA was used as the electrolyte solution, the photocurrent intensity of the GR–CdS/ITO electrode with light on and off increased greatly compared with that of the CdS/ITO electrode (Fig. 4A), indicating that the incorporation of GR did efficiently enhance the photoelectric responses of the GR–CdS nanocomposites. Moreover, the GR–CdS/ITO electrode shows a strong and rather stable photocurrent response in phosphate buffer solution (PBS, pH 7.4) containing 0.1 M AA, even after the GR–CdS/ITO electrode was stored for two months (Fig. 4B).

Due to the biological importance of glutathione, GSH was used as an antioxidant model molecule, upon addition of 500 μmol L^{-1} GSH, the photocurrent of GR–CdS/ITO electrode increased to 4.18 μA and remained steady (Fig. 3A, curve c). The

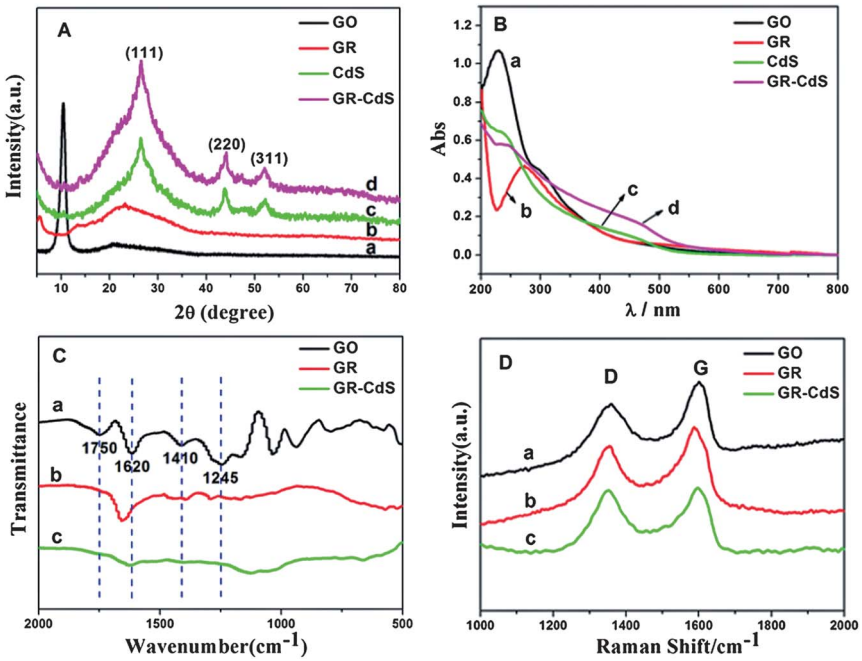

Fig. 2 (A) XRD patterns and (B) UV-vis spectra of (a) GO, (b) GR, (c) free CdS, and (d) GR–CdS nanocomposites. (C) FT-IR spectra and (D) Raman spectra of (a) GO, (b) GR and (c) GR–CdS nanocomposites.

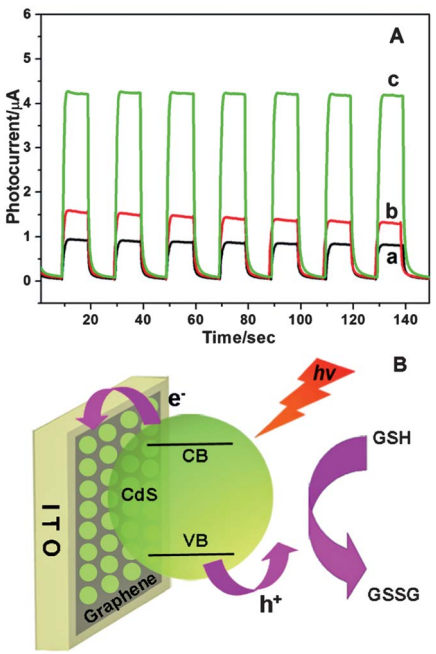

Fig. 3 (A) Photocurrent responses of (a) CdS/ITO, (b) GR–CdS/ITO in 0.1 M pH 7.0 PBS 0 V, and (c) photocurrent responses of GR–CdS/ITO in 0.1 M pH 7.0 PBS in the presence of 500 μmol L^{-1} GSH at 0 V to a light excitation at 470 nm. (B) Schematic illustration of photoelectrochemical process for oxidation of GSH at GR–CdS modified ITO electrode.

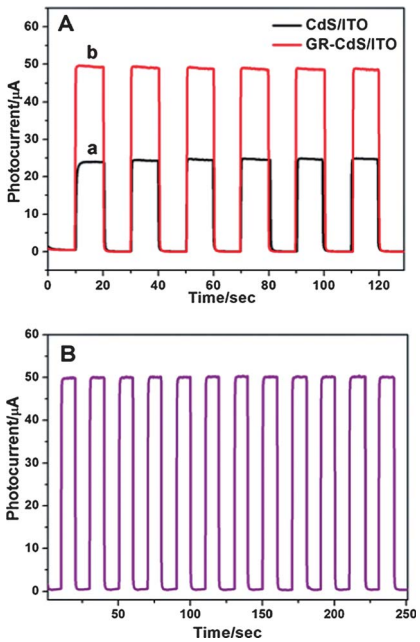

Fig. 4 (A) Photocurrent responses of (a) CdS/ITO, (b) GR–CdS/ITO electrode in 0.1 M pH = 7.0 PBS containing 0.1 M AA with light on and off. The applied potential was 0 V and the light wavelength was 470 nm. (B) Time-based photocurrent responses of the GR–CdS/ITO electrode measured in 0.1 M pH = 7.0 PBS containing 0.1 M AA with light on and off after being stored for two months.

increase of photocurrent was attributed to the oxidization of GSH by the photogenerated holes, avoiding electron–hole recombination effectively. The photoelectrochemical process of the GR–CdS film for GSH oxidation is proposed in Fig. 3B. Upon irradiation with light, CdS NCs were excited and underwent charge separation to yield electrons (e^-) and holes (h^+). Bulk CdS has a band-gap of 2.42 eV; however, the band-gap energy of CdS NCs should be higher than 2.42 eV due to the quantum confinement regime. Since the energy levels of the conduction band of GR and ITO are lower than that of CdS,[43–45]

the electron transfer from the conduction band of CdS NCs to GR and then from GR to ITO are an energetically favorable process. Due to the superior electrical conductivity of GR, it serves as an excellent electron-transport matrix to capture electrons and transport electrons from excited CdS to ITO rapidly, avoiding electron–hole recombination effectively, resulting in a much more sensitive response to light on and off. Thus, the favorable band energy, good distribution of CdS and strong coupling of CdS and GR efficiently enhance the photoelectric responses of the GR–CdS nanocomposites. Because the light absorption of GR can adversely affect the excitation of CdS nanoparticles, leading to a sharp decrease of photocurrent, the ratio of GR and CdS should be controlled carefully. In this work, we have tried to decrease and increase the GR loadings, but both lead to photocurrent decrease. Hence, the ratio of GR and CdS as the optimum condition was chosen. At this ratio, the GR–CdS/ITO electrode shows a stronger and stable photocurrent that is suitable for the fabrication of biosensors. In the presence of GSH, it served as the electron donor (hole scavenger) and sacrificial reagent can transfer electrons to the holes located on the excited state of CdS, avoiding electron–hole recombination effectively, leading to a sharp increase of the photocurrent. During this process, GSH was oxidized to glutathione disulfide (GSSG).

Condition optimization

To optimize the experimental conditions for GSH measurement, the effects of applied potential and the excitation wavelength were investigated. Applied potential is an important factor relevant to the photocurrent response. As seen in Fig. 5A, upon addition of 500 μmol L^{-1} GSH, with an increase of potential from −0.2 V to 0 V (*vs.* Ag/AgCl), the photocurrent increased sharply, and as the potential increased from 0 V to +0.3 V, the photocurrent decrease gradually. Therefore, 0 V was selected as the applied potential for the determination of GSH. A negative potential (−0.2 V, −0.1 V) can inhibit the electron transfer from GR–CdS to the electrode, which may lead to electron–hole recombination. In the potential range from 0 to 0.3 V, the responses showed a slight decrease with the increase of the applied potential. The increase of the positive potential could cause electrochemical oxidization of GSH, thus the GSH (hole scavenger) decreased, resulting in the decrease of the photocurrent. The potential in this method was more negative than that of +0.2 V for the photoelectrochemical oxidation of GSH at the FeTPPS–TiO_2-modified ITO electrode.[46] The low applied potential was beneficial to the elimination of interference from other reductive species that coexisted in the real samples.

The irradiation wavelength is another significant factor that is relevant to the photocurrent response. As shown in Fig. 5B, upon addition of 500 μmol L^{-1} GSH, the photocurrent increased as the exciting wavelength was increased from 420 nm to 470 nm at the applied potential of 0 V. Afterward, the photocurrent quickly decreased. Moreover, consider that biomolecules may suffer from irradiation with light of excessively short wavelength. Thus, 470 nm was chosen for the photoelectrochemical biosensing of GSH.

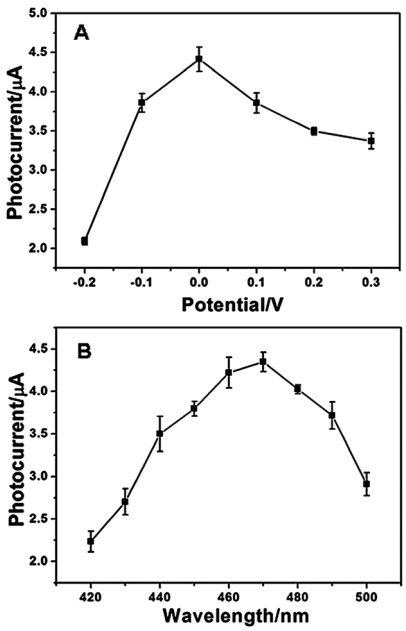

Fig. 5 Effects of (A) applied potential (*vs.* Ag/AgCl) and (B) excitation wavelength on photocurrent responses of GR–CdS/ITO electrode in 0.1 M pH 7.0 PBS containing 500 μmol L^{-1} GSH.

Photoelectrochemical detection of GSH

The photocurrent–time curve of the GR–CdS/ITO electrode clearly shows the rapid response of the modified electrode to GSH at an applied potential of 0 V (Fig. 6A). Under the optimal conditions, a good linear relationship between the photocurrent increase value and logarithmic value of GSH concentration could be obtained in the range of 0.01–1.5 mmol L^{-1} with a detection limit of 3 μmol L^{-1} at 3σ, which was much lower than the detection limit reported for a previous photoelectrochemical sensor.[46] The linear regression equation was i (μA) = −0.2329 + 1.6044logC_{GSH} (μmol L^{-1}) with a correlation coefficient of 0.9986. The linear response range was wider than those of other strategies for the quantitative detection of GSH.[12,46–48] Furthermore, the detection limit of 0.003 mmol L^{-1} was rather lower than the earlier report,[12,46–48] achieving the sensitive detection for GSH. Hence, the proposed photoelectrochemical biosensor based on GR–CdS nanocomposites showed promising application in the sensitive monitoring of GSH over a wide concentration range.

Interference and assays of real sample

GSH is the most abundant thiol species in the cytoplasm and the major reducing agent in biochemical processes. It is often used as the auxiliary for the chemotherapy of cancer. Hence, the effects of anticancer drugs as interfering species on the photoelectrochemical biosensing response of GSH were investigated. For example, as is shown in Fig. 6B, etoposide, actidione, cisplatin and adriamycin did not interfere with the photoelectrochemical response of GSH. In the presence of interferents, the photocurrent responses remained almost unchanged. Thus, the proposed photoelectrochemical biosensor based on the

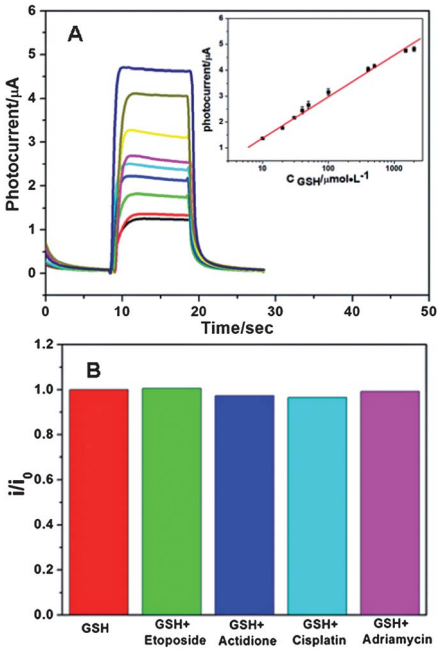

Fig. 6 (A) Photocurrent responses of GR–CdS/ITO electrode in 0.1 mol L^{-1} pH 7.0 PBS in the presence of 0, 10, 20, 30, 40, 50, 100, 500, and 1500 μmol L^{-1} GSH (from bottom to top) at 0 V to light excitation at 470 nm. Inset: linear calibration curve. (B) Photocurrent ratio i/i_0 of GR–CdS/ITO electrode in 0.1 M pH 7.0 PBS containing GSH in the presence of various interferent species (etoposide, actidione, cisplatin and adriamycin) at 0 V to light excitation at 470 nm (i_0 and i are the photocurrents of the GR–CdS/ITO electrode before and after addition of interferents).

GR–CdS nanocomposites had an excellent specificity for the detection of GSH in samples with anticancer drugs.

Glutathione-containing drugs are widely applied in clinics, significantly to strengthen immunity, cancer therapies, *etc.*, and play a part in the treatment of human immunodeficiency virus (HIV).[49] Hence, real sample assays about glutathione-containing drugs are also expected. The proposed sensor could realize the direct, sensitive, and continuous detection of the glutathione-containing drug Isethion (5 mL/100 mg, Tathion eye drops, Japan). The concentration of reduced glutathione in Isethion was detected with the proposed photoelectrochemical biosensor to be 62.35 ± 0.05 mmol L^{-1} (five measurements) without any need of sample pretreatment except for appropriate dilution. This value was consistent with the 65 mmol L^{-1} (5 mL/100 mg) value given in the instructions of Isethion, indicating acceptable accuracy of the photoelectrochemical biosensor. This photoelectrochemical biosensor reflected its actual application in glutathione-containing drug detection, indicating its potentiality in physiological assays.

Conclusion

In this work, a novel photoelectrochemical biosensing platform for GSH detection was developed using newly synthesized GR–CdS nanocomposites, which were prepared by a facile, one-step, aqueous reaction. The GR–CdS heteronanostructure inherited the excellent electron transport advantage of GR and facilitated the spatial separation of charge carriers, therefore resulting in the enhanced and stable photocurrent, and making it a promising candidate for the development of a photoelectrochemical biosensor. Using GSH as a hole scavenger, the fast photoelectronic communication among GSH, CdS, GR sheet and ITO electrode led to a novel strategy for the photoelectrochemical detection of GSH. The proposed photoelectrochemical biosensor showed good analytical performance, such as low applied potential, rapid response, wide linear range, and rather low detection limit. Moreover, it showed excellent specificity for excluding the interference of other anticancer drugs and acceptable accuracy in real sample detection. The GR–CdS nanocomposites with excellent photovoltaic properties can be an efficient candidate material for the construction of other high-performance photovoltaic devices.

Acknowledgements

We are grateful to the support of '973' Program (No. 2011CB933502), the International S&T Cooperation Projects of China (2010DFA42060), and National Natural Science Foundation of China (21075061, 21105050).

References

1 A. Meister and M. E. Anderson, *Annu. Rev. Biochem.*, 1983, **52**, 711–760.
2 M. Novak and J. Lin, *J. Am. Chem. Soc.*, 1996, **118**, 1302–1308.
3 R. Franco, M. I. Panayiotidis and J. A. Cidlowski, *J. Biol. Chem.*, 2007, **282**, 30452–30465.
4 R. J. Singh, *J. Lab. Clin. Med.*, 2002, **140**, 380–381.
5 Y. Li, P. Wu, H. Xu, H. Zhang and X. H. Zhong, *Analyst*, 2011, **136**, 196–200.
6 G. G. Huang, M. K. Hussain, X. X. Han and Y. Ozaki, *Analyst*, 2009, **134**, 2468–2474.
7 P. K. Sudeep, S. T. S. Joseph and K. G. Thomas, *J. Am. Chem. Soc.*, 2005, **127**, 6516–6517.
8 Y. Fujikawa, Y. Urano, T. Komatsu, K. Hanaoka, H. Kojima, T. Terai, H. Inoue and T. Nagano, *J. Am. Chem. Soc.*, 2008, **130**, 14533–14543.
9 W. Lin, L. Yuan, Z. Cao, Y. Feng and L. Long, *Chem.–Eur. J.*, 2009, **15**, 5096–5103.
10 J. Liu, C. Bao, X. Zhong, C. Zhao and L. Zhu, *Chem. Commun.*, 2010, **46**, 2971–2973.
11 Y. H. Ahn, J. S. Lee and Y. T. Chang, *J. Am. Chem. Soc.*, 2007, **129**, 4510–4511.
12 G. G. Huang, X. X. Han, M. K. Hossain and Y. Ozaki, *Anal. Chem.*, 2009, **81**, 5881–5888.
13 G. L. Wang, J. J. Xu, H. Y. Chen and S. Z. Fu, *Biosens. Bioelectron.*, 2009, **25**, 791–796.
14 G. L. Wang, P. P. Yu, J. J. Xu and H. Y. Chen, *J. Phys. Chem. C*, 2009, **113**, 11142–11148.
15 C. Stoll, S. Kudera, W. J. Parak and F. Lisdat, *Small*, 2006, **2**, 741–743.
16 Y. T. Long, C. Kong, D. W. Li, Y. Li, S. Chowdhury and H. Tian, *Small*, 2011, **7**, 1624–1628.
17 N. Haddour, J. Chauvin, C. Gondran and S. Cosnier, *J. Am. Chem. Soc.*, 2006, **128**, 9693–9698.
18 A. Ikeda, M. Nakasu, S. Ogasawara, H. Nakanishi, M. Nakamura and M. Kikuchi, *Org. Lett.*, 2009, **11**, 1163–1166.
19 Q. M. Shen, X. M. Zhao, S. W. Zhou, W. H. Hou and J. J. Zhu, *J. Phys. Chem. C*, 2011, **115**, 17958–17964.
20 X. N. Wang, H. J. Zhu, Y. M. Xu, H. Wang, Y. Tao, S. K. Hark, X. D. Xiao and Q. Li, *ACS Nano*, 2010, **4**, 3302–3308.
21 Y. Tak, S. J. Hong, J. S. Lee and K. Yong, *J. Mater. Chem.*, 2009, **19**, 5945–5951.
22 J. H. Bang and P. V. Kamat, *Adv. Funct. Mater.*, 2010, **20**, 1970–1976.
23 I. Robel, B. A. Bunker and P. V. Kamat, *Adv. Mater.*, 2005, **17**, 2458–2463.

24 L. Sheeney-Haj-Khia, B. Basnar and I. Willner, *Angew. Chem., Int. Ed.*, 2005, **44**, 78–83.
25 L. Sheeney-Haj-Ichia, J. Wasserman and I. Willner, *Adv. Mater.*, 2002, **14**, 1323–1326.
26 S. Banerjee and S. S. Wong, *Nano Lett.*, 2002, **2**, 195–200.
27 S. Ravindran, S. Chaudhary, B. Colburn, M. Ozkan and C. S. Ozkan, *Nano Lett.*, 2003, **3**, 447–453.
28 A. K. Geim and K. S. Novoselov, *Nat. Mater.*, 2007, **6**, 183–191.
29 V. Yong and J. M. Tour, *Small*, 2010, **6**, 313–318.
30 J. F. Yan, Q. Ye, X. L. Wang, B. Yu and F. Zhou, *Nanoscale*, 2012, **4**, 2109–2116.
31 H. X. Chang, X. J. Lv, H. Zhang and J. H. Li, *Electrochem. Commun.*, 2010, **12**, 483–487.
32 A. N. Cao, Z. Liu, S. S. Chu, M. H. Wu, Z. M. Ye, Z. W. Cai, Y. L. Chang, S. F. Wang, Q. H. Gong and Y. F. Liu, *Adv. Mater.*, 2010, **22**, 103–106.
33 X. M. Zhao, S. W. Zhou, L. P. Jiang, W. H. Hou, Q. M. Shen and J. J. Zhu, *Chem.–Eur. J.*, 2012, **18**, 4974–4981.
34 K. Jasuja and V. Berry, *ACS Nano*, 2009, **3**, 2358–2366.
35 X. J. Zhou, J. L. Zhang, H. X. Wu, H. J. Yang, J. Y. Zhang and S. W. Guo, *J. Phys. Chem. C*, 2011, **115**, 11957–11961.
36 J. L. Lyon, D. A. Fleming, M. B. Stone, P. Schiffer and M. E. Williams, *Nano Lett.*, 2004, **4**, 719–723.
37 W. S. Hummers and R. E. Offeman, *J. Am. Chem. Soc.*, 1958, **80**, 1339.
38 T. Nakajima, A. Mabuchi and R. Hagiwara, *Carbon*, 1988, **26**, 357–361.
39 X. Wang, L. J. Zhi, N. Tsao, J. L. Tomovic and K. Mullen, *Angew. Chem., Int. Ed.*, 2008, **47**, 2990–2992.
40 H. L. Guo, X. F. Wang, Q. Y. Qian, F. B. Wang and X. H. Xia, *ACS Nano*, 2009, **3**, 2653–2659.
41 Y. C. Si and E. T. Samulski, *Nano Lett.*, 2008, **8**, 1679–1682.
42 Y. X. Xu, H. Bai, G. W. Lu, C. Li and G. Q. Shi, *J. Am. Chem. Soc.*, 2008, **130**, 5856–5860.
43 W. Zhang, Y. R. Shi, L. B. Gan, C. H. Huang, H. X. Luo, D. G. Wu and N. Q. Li, *J. Phys. Chem. B*, 1999, **103**, 675–681.
44 R. Gill, F. Patolsky, E. Katz and I. Willner, *Angew. Chem., Int. Ed.*, 2005, **44**, 4554–4557.
45 C. X. Guo, H. B. Yang, Z. M. Sheng, Z. S. Lu, Q. L. Song and C. M. Li, *Angew. Chem., Int. Ed.*, 2010, **49**, 3014–3017.
46 W. W. Tu, Y. T. Dong, J. P. Lei and H. X. Ju, *Anal. Chem.*, 2010, **82**, 8711–8716.
47 Y. Wang, J. Lu, L. H. Tang, H. X. Chang and J. H. Li, *Anal. Chem.*, 2009, **81**, 9710–9715.
48 Z. Y. Yao, X. L. Feng, C. Li and G. Q. Shi, *Chem. Commun.*, 2009, 5886–5888.
49 W. A. Kleinman and J. P. Richie, *Biochem. Pharmacol.*, 2000, **60**, 19–29.